Sensor-based optimal delineation of management zones for plant and soil integration

André Victor Hereman[1]; João Vítor Fiolo Pozzuto[2]; Lucas Rios do Amaral[3]

[1] Agricultural Engineering Student, Interdisciplinary Group on Precision Agriculture Technology (GITAP), Feagri/Unicamp, Brazil

[2] PhD Student, Agricultural Engineer, Nuclear Instrumentation Laboratory, CENA/USP, Brazil

[3] Professor, Agronomist, Interdisciplinary Group on Precision Agriculture Technology (GITAP), Feagri/Unicamp, Brazil

A paper from the Proceedings of the
17th International Conference on Precision Agriculture and 11th Brazilian Congress on Precision and Digital Agriculture
13-15 July 2026
Porto Alegre, Brazil

ABSTRACT.
Strategies for mapping management zones (MZs) use proximal and orbital sensors to optimize use and promote sustainable development. Proximal sensors can infer, among other variables, apparent electrical conductivity (ECa), while orbital sensors provide synthetic soil images (SYSI), digital elevation model (DEM), and different color-composition images of soil and plant canopies. However, the literature does not provide clear evidence on the efficiency of these measurements, individually and jointly, in reducing the internal variability of MZs when pursuing a dual simultaneous objective: accounting for plant and soil variability. Therefore, this study aimed to determine the optimal combination of data sensors for delineating MZs and select the one that represents the lowest internal variance. The study was conducted in a 103-ha agricultural field located in São Paulo State, Brazil, cultivated with soybean in summer and sorghum or oats in winter. A seven-harvest (2020-2024) composite map was generated via arithmetic averaging and PCA. Furthermore, a Soil Nutrient Variability Index (SNVI) was calculated by MULTISPATI-PCA. ECa data were collected using an on-the-go EM38-MKII sensor at shallow and deep layers. Orbital data were obtained, including an DEM from Japan Aerospace Exploration Agency (JAXA) and SYSI from Sentinel-2 time-series imagery, from which RGB images were extracted and converted to the HSI color space. All datasets were co-located and analyzed using bivariate spatial autocorrelation (Moran's I). Furthermore, the following scenarios were created using different variables without a previous analysis and grounded on Moran's I to delineate MZs using MULTISPATI-PCA: all gathered variables (MZ1); all SYSI bands (MZ2); the hue, saturation, and intensity components (MZ3); ECa from both depth (MZ4); DEM (MZ5); ECa75 (MZ6); ECa75 and

The authors are solely responsible for the content of this paper, which is not a refereed publication. Citation of this work should state that it is from the Proceedings of the 17th International Conference on Precision Agriculture and 11th Brazilian Congress on Precision and Digital Agriculture. EXAMPLE: Hereman, A.V.; Pozzuto, J.V.F.; Amaral, L.R. (2026). Sensor-based optimal delineation of management zones for plant and soil integration. In Proceedings of the 17th International Conference on Precision Agriculture and 11th Brazilian Congress on Precision and Digital Agriculture (unpaginated, online). Monticello, IL: International Society of Precision Agriculture and Brazilian Congress on Precision and Digital Agriculture.

DEM (MZ7); ECa75, DEM, and NIR band (MZ8); ECa75, DEM, and red edge band (MZ9); ECa75, DEM, and SWIR1 (MZ10); ECa75, DEM, SWIR1, and hue (MZ11); ECa75, DEM, SWIR1, and intensity (MZ12); ECa75, DEM, SWIR1, and saturation (MZ13); all filtered variables (i.e., excluding non-significant and highly collinear variables) (MZ14); all filtered variables without saturation (MZ15); all filtered variables without DEM (MZ16); and all filtered variables without ECa75 (MZ17). The resulting MZs were statistically compared using variance reduction (VR%), assuming the mean and PC1 yield data and the SNVI as references. Then, an average VR% was calculated from the three references. The results showed that using data from different sources and filtering them improved the VR% from 2, 3, and 4 zones when compared to MZs generated by only one data source. For 2, 3, and 4 zones, integrating data from proximal and orbital sensors reduced the internal variance by up to 56.6% (MZ7), 57.3% (MZ10), and 62,3% (MZ14), respectively, being a good performance in the variance reduction. Thus, considering the preservation of yield and soil characteristics, followed by a minimizing of internal variance, selecting data that represent different soil properties is a good approach to account for both plant and soil variability in the management zones delineation.

KEYWORDS.
Soil health, Sensor fusion, Digital soil mapping, Site-specific management, Pedometrics.

INTRODUCTION

Soil spatial variability mapping is one of the most widely adopted objectives of Precision Agriculture (PA) (Molin & Tavares, 2019), which, in turn, is a management strategy to improve the sustainability of agricultural production by accounting for temporal and spatial variability (ISPA, 2024). Usually, soil variability mapping is conducted using georeferenced samples collected in a grid that shall be dense enough to capture the short-range spatial dependence of the target properties. In tropical soils (such as brazilians), the density can be over 1 sample per hectare, depending on the target property (Cherubin et al., 2022). This conventional approach is known to be time- and resource-consuming, limiting the proper characterization of soil variability. Regarding alternatives to conventional sampling, two are among the most widely used. The first is the use of sensors, related to soil formation, that infer (generally indirectly) soil variability in a much denser and cheaper way, an approach often known as digital soil mapping (DSM) (McBratney et al., 2003). The second approach is to subdivide the area into homogeneous areas that are sufficiently similar within them, allowing not only for uniform management but also for simple soil collection, a process known as management zone delineation (Nawar et al., 2017). For soil sampling, since the subdivisions are homogeneous, a single composite sample can be collected for each subdivision by aggregating subsamples around the management zone (MZ) and mixing them into a single sample, which can then be sent to a laboratory (Nawar et al., 2017).

For MZ delineation, various approaches have been studied, including algorithms for clustering the area and input layers. The latter generally comprises information from (individual or combined) soil, vegetation, topography, and sensing. Among these, sensing information is particularly advantageous for providing high-resolution, continuous, and cost-effective data over large areas (Adamchuk et al., 2004; Molin & Tavares, 2019). For this study, the apparent electrical conductivity (ECa) (Tavares et al., 2025), the synthetic soil image (SYSI) (Demattê et al., 2018), and the digital elevation model (DEM) (Peralta & Costa, 2013) are highlighted.

As a proxy for several agronomic attributes, apparent electrical conductivity (ECa) reflects the soil's capacity to conduct electrical current and responds directly to variations in texture, moisture, organic matter, and salinity (Corwin & Lesch, 2005). The measurement is considered 'apparent' because it records the bulk conductivity directly in the field, integrating the complex electrical pathways that occur across the solid, liquid, and solid-liquid phases of the soil matrix (Corwin & Lesch, 2005). For field-scale mapping, ECa is typically surveyed using electromagnetic induction (EMI) sensors. This equipment operates by projecting a primary alternating electromagnetic field into the ground through a transmitting coil, which in turn induces a secondary field within the soil profile. A receiving coil then captures the combined fields, enabling continuous, high-density acquisition of ECa data without soil disturbance (Shirzaditabar & Heck, 2022).

Not only can proximal sensors be used, but also orbital ones. However, the widespread use of no-tillage systems, especially in Brazil, often limits the availability of clean, bare soil satellite imagery. As an alternative, the synthetic soil image (SYSI) approach overcomes this limitation by utilizing a historical database of satellite data (e.g., Sentinel-2). Using specific segmentation criteria, such as the GEOS3 methodology (Demattê et al., 2018), isolated bare-soil pixels collected over time are integrated into a single synthetic image, revealing the area's spatial variability from spectral bands without requiring conventional soil preparation. Furthermore, the Digital Elevation Model (DEM) provides essential topographic information via digital terrain representation (Hengl & MacMillan, 2009). These sensor-derived layers have been extensively applied as base information for delineating MZ (Pentoś et al., 2021; Oldoni et al., 2025). MZs are defined as sub-regions of a field that exhibit similar combinations of yield-limiting factors, allowing for uniform, site-specific management within each unit (Nawar et al., 2017). However, optimal MZ delineation must account for both the underlying soil properties and the actual plant response to these factors. Currently, there is insufficient evidence to demonstrate that soil sensing techniques alone can fully capture this complex soil-plant interaction.

OBJECTIVES

Therefore, to overcome the limitations of single-layer approaches in Precision Agriculture, this study aimed to evaluate the integration of proximal soil sensing (ECa), orbital data (SYSI), and topography (DEM) for the delineation of management zones, hypothesizing that the fusion of these distinct sensing layers more accurately captures the soil-plant interaction and effectively minimizes the within-zone variability of both soil and plant attributes

MATERIAL AND METHODS

In this work it was used data from the database of the Interdisciplinary Group of Precision Agriculture Technology (Grupo Interdisciplinar de Tecnologia em Agricultura de Precisão - GITAP) at FEAGRI/UNICAMP. The study was conducted on a 103 ha area (Figure 1) at the São José Farm in Cosmópolis, São Paulo, which has predominantly Ferralsols (corresponding to *Latossolo Vermelho distrófico*), with some regions of Gleysols (*Gleissolo Háplico*). In this, a direct planting system has been used since 2019, succeeding soy in the harvest period and sorghum and oat during the winter crop.

Figure 1: São José Farm map, localized in Cosmópolis - SP.

Plant information was measured by a harvester's yield monitoring system, generating a yield map across the area. It provided a map series from seven consecutive harvests, minimizing the influence of external factors that affect crop yield in individual harvest analyses, such as localized pest infestations or operational errors. Thus, the use of a map series is preferred over a single harvest, which could not represent soil variability across the area. This map series was generated from the soy harvests in 2020-2021, 2021-2022, 2022-2023, and 2023-2024, and the winter crops in 2021 and 2023, for sorghum, and in 2022 for oat. All this yield data was normalized using the min-max method to reduce the influence of external factors and make it comparable across crops and years (Molin et al., 2015), despite differences in yield levels across crops (soybean, sorghum, and oat) and years. Then, the normalized yield data were interpolated using ordinary kriging (OK) within the area shapefile at a 5-meter resolution, resulting in 7 individual yield maps. Lastly, these maps were linked using two methods: arithmetic mean for each pixel and principal component analysis (PCA), selecting, in this case, the first component (PC1), which represents more than 70% of the variability and normalizing it (Figure 2).

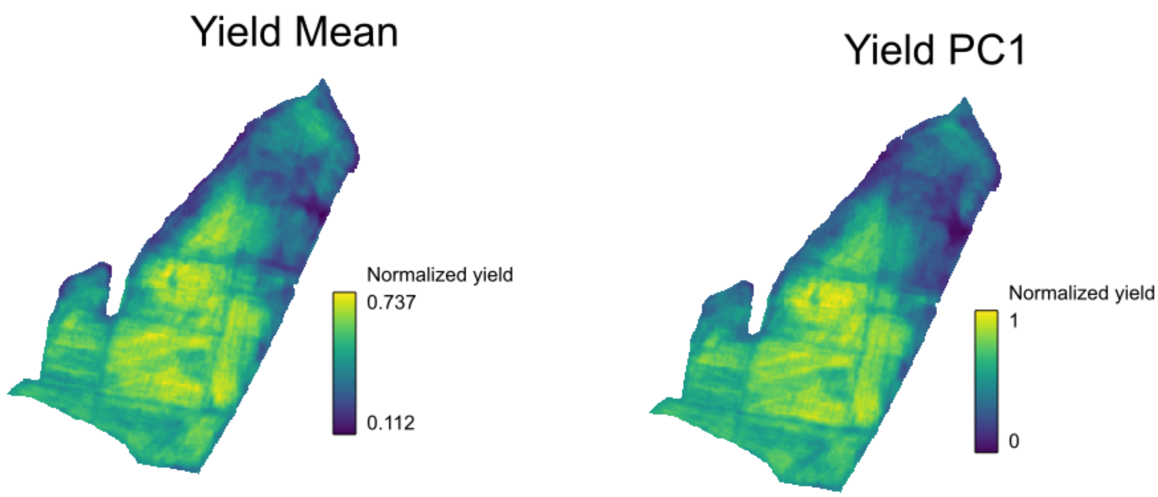

Figure 2: Yield productivity maps generated by mean and PC1.

Also, soil samples were collected in 2023 as part of a high-density sampling scheme, with 6 samples per hectare, totaling 656 samples in the 0-0.2 m depth layer. For each soil sample, 6 sub-samples were randomly collected within a 5-meter radius of the sampling site. After these samples were taken to a commercial laboratory for chemical analysis. The measured nutrients were calcium (Ca), phosphorus (P), magnesium (Mg), and manganese (Mn), and they were used to calculate a soil nutrient variability index (SNVI), which was done using the MULTISPATI-PCA method that consists of verifying the relations among the nutrients and their spatial correlation (Dray et al., 2008). To represent the variance appropriately, were select the set of components with the variance $\geq$ 70% (Table 1). For this work, PC1 and PC2 were selected. Furthermore, we used the relation with the 4 nearest neighbors (K-nearest neighbors) of each site to create a weighting matrix, with row sums standardized. Then, the MULTISPATI was performed to calculate the weighted EVs, with their sum set to 1, and finally, the SNVI was calculated by multiplying the weighted EVs matrix by the spatial components (SC) matrix generated from the selected PCs. To maintain the precision of the soil variability data, this data was not interpolated. The SNVI was normalized using the min-max method, projected onto the area (Figure 3), and visually represents nutrient behavior across the São José farm.

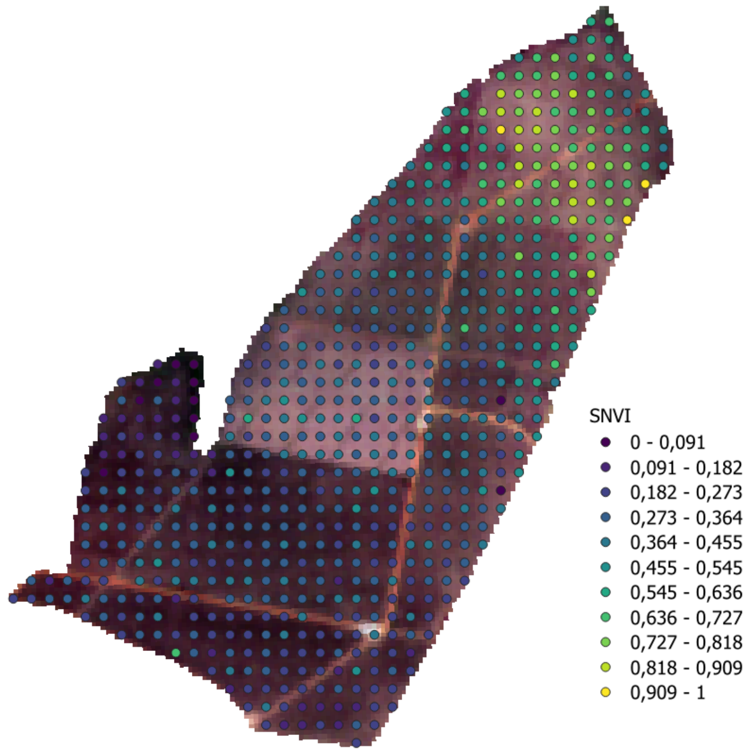

Figure 3. Soil sampling grid and SNVI for each data point.

Table 1. Results of PCA of nutrient variance on the São José Farm.

	PC1	**PC2**	PC3	PC4
Eigenvalue	**2.31**	**1.08**	0.38	0.23
Proportion of Variance	0.58	0.27	0.10	0.06
Cumulative Proportion	**0.58**	**0.85**	0.94	1

Bolded components were selected for SNVI calculation.

Proximal sensor data were obtained with EM38 MKII (Geonics, Ontario, Canada), which is an electromagnetic induction sensor (EMI), pulled by a quadricycle, and can gather real time and high-density data (100 samples per hectare). This sensor simultaneously inferred ECa at two depth layers: from 0 to 0.375 m (ECa375) and to 0.75 m (ECa75), generating two data points at the same coordinate. Also, these data were interpolated by OK at a 5-meter resolution, resulting in 2 continuous ECa maps for both layers.

Meanwhile, the orbital sensor data were gathered using Google Earth Engine (GEE). The SYSI were calculated by the Geospatial Soil Sensing System (GEOS3) algorithm (Demmatê *et al*., 2018) for the whole Sentinel-2 historical serie, searching for images between 2018/10/15 and 2024/12/07, during july to december, with less than 10% of cloud cover, 0.25 of NDVI a VSWIR until 0.9, increasing the probability of select soil pixels to compose the image for 7 bands (blue, green, red, NIR, red edge, SWIR1, and SWIR2) (Silvero et al., 2021; Demattê *et al*., 2025). Moreover, based on the generated image, an algorithm was used to convert the RGB colors to HSI (Bejarano *et al*., 2026), which uses hue, saturation, and intensity in the composition to create a color, and it showed effectiveness in detecting soil spatial variability (Pozzuto et al., 2026). Also, the DEM data were obtained from the Japan Aerospace Exploration Agency (JAXA), with a spatial resolution of 12.5 m. As with yield and ECa, the orbital sensor data were interpolated to a common spatial resolution to enable comparison.

With the interpolated data of the yield, proximal, and orbital, and the point data of the SNVI, it was calculated the spatial correlation between these variables was calculated using Bivariate Moran (Figure 4), which allowed us to select significant variables ($p<0.05$) variables to create MZ that are complementary to each other, decreasing the redundant information. First, we selected scenarios including all gathered variables (MZ1), all SYSI bands (MZ2), and the hue, saturation, and intensity components (MZ3). Then, analyzing the Moran Bivariate results, we also selected variables with the strongest correlations with yield and SNVI, and tested them individually and in combination, integrating data that represent different aspects of the soil. Thereby, were made the following scenarios: ECa from both depth (MZ4); DEM (MZ5); ECa75 (MZ6); ECa75 and DEM (MZ7); ECa75, DEM, and NIR band (MZ8); ECa75, DEM, and red edge band (MZ9); ECa75, DEM, and SWIR1 (MZ10); ECa75, DEM, SWIR1, and hue (MZ11); ECa75, DEM, SWIR1, and intensity (MZ12); and ECa75, DEM, SWIR1, and saturation (MZ13). In addition, we selected all variables and removed blue band, red edge band, and hue band for their correlation was not significant simultaneously, to yield mean, yield PC1 and SNVI, and removed the ECa375 for it was correlated with EC75 in 0.94 and removed SWIR2 because it was correlated to SWIR1 in 0.88. Both ECa375 and SWIR2 were chosen for removal because they had lower correlations with yield mean, yield PC1, and SVNI than ECa75 and SWIR1. Then, we tested the following scenarios: all filtered variables (MZ14); all filtered variables without saturation (MZ15); all filtered variables without DEM (MZ16); and all filtered variables without ECa75 (MZ17).

After this, the z-score was applied to the individual scenarios and to MULTISPATI-PCA for the combinations (Oldoni et al., 2025). Regarding MULTISPATI-PCA, the selected number of components explained at least 70% of the variance. Afterward, the fuzzy c-means clustering method was applied (Córdoba et al., 2016). To delineate the MZ, the optimal number of zones was determined using the fuzziness performance index (FPI), modified partition entropy (MPE), and silhouette width (SW) (OLDONI et al., 2025), selecting 2, 3, and 4 zones. These zones were smoothed using a modal filter via the Precision Zones plugin in QGIS and, in some cases, first using a median filter (OLDONI et al., 2025), which was efficient at removing small regions without modifying larger regions that could be important for representing spatial variability. The smoothing was done until the remaining regions had approximately 1 ha. Thereafter, the variance reduction (VR%) of mean and yield PC1, as well as the SNVI, was calculated by equation 1 for each zone (2, 3, and 4) from MZs and were compared with each other (Figures 5, 6, and 7).

$$VR\% = \frac{1 - WV}{TV}(100) \qquad \text{(Equation 1)}$$

With WV as the weighted productivity zone by the area, and TV as the total variance of the area.

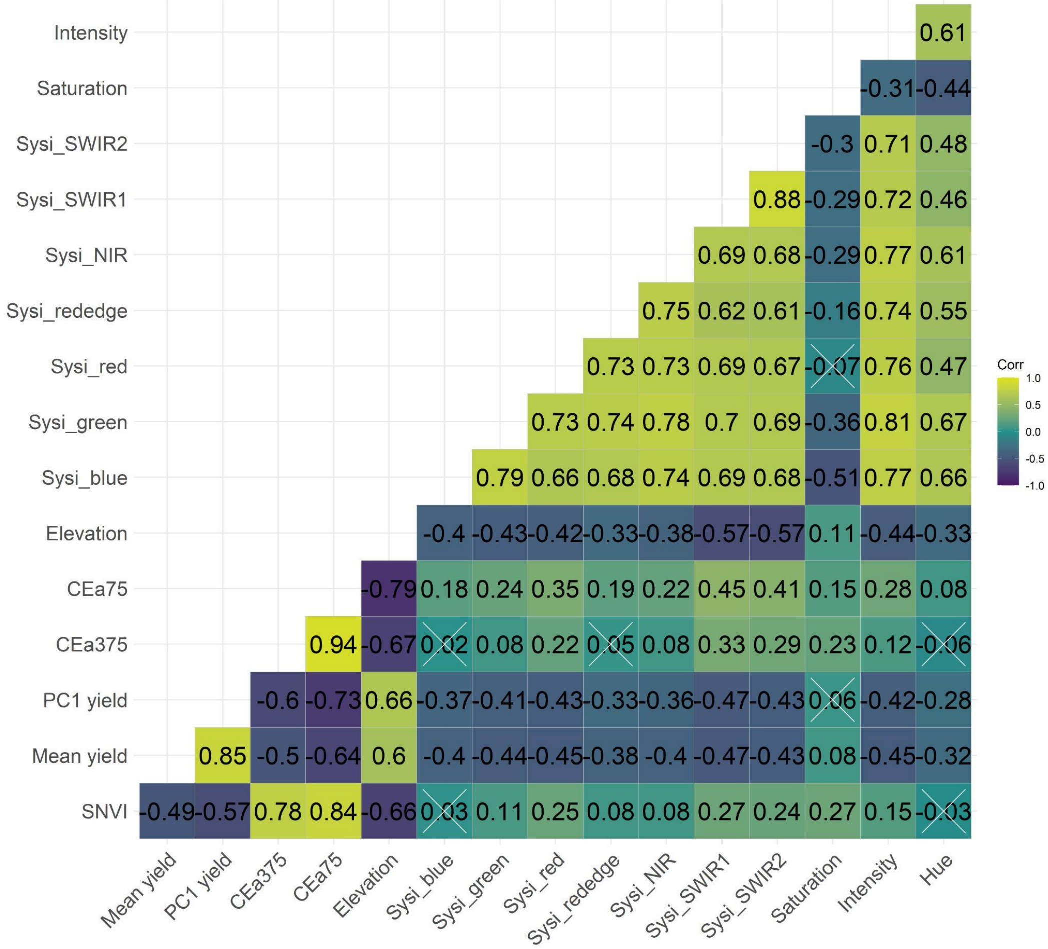

Figure 4. Correlation Matrix by Bivariate Moran between all variables. Cells marked with ‘X’ indicate that the Moran correlation was not significant at the 5% level.

RESULTS AND DISCUSSION

The variance reduction (VR%) for the yield mean (Figure 5) was good (40%-70%) across most scenarios, according to Melo et al. (2025). These results are consistent with those found in the literature (Nawar et al., 2017). Combining ECa75, DEM, and NIR band (MZ8) yielded the best result for 2 zones, reducing the internal variance in yield by 58.1%. For 3 zones, the combination of ECa75, DEM, and SWIR1 (MZ10) was the best, reducing yield variance by 54.2%. Moreover, using all filtered variables (MZ14) had the highest VR% for 4 zones (58.7%). The synergy of data fusion from topographic, remote, and proximal sensing aligns with the results of Oldoni et al. (2025), who found that EVI, ECa, elevation, and soil information together were the optimal layers for management zone delineation. Nevertheless, using just one variable, in this case only DEM (MZ5), presented similar results with 55.1%. This supports the fundamental role of topography as a primary driver of soil formation (McBratney et al., 2003). Because terrain attributes govern pedogenetic processes and the spatial distribution of soil properties, the DEM alone can serve as a robust proxy to delineate MZ. Consequently, in some scenarios, the DEM can explain a large portion of yield variability (Kravchenko & Bullock, 2000) without additional sensor data. Also, not making an analysis and/or filtering on the data presented good, similar results, minimizing the yield within-zone variance by 55.4%. Overall, for the yield mean, according to VR%, the best scenario to reduce internal variance across the zones is to adopt the MZ14 configuration.

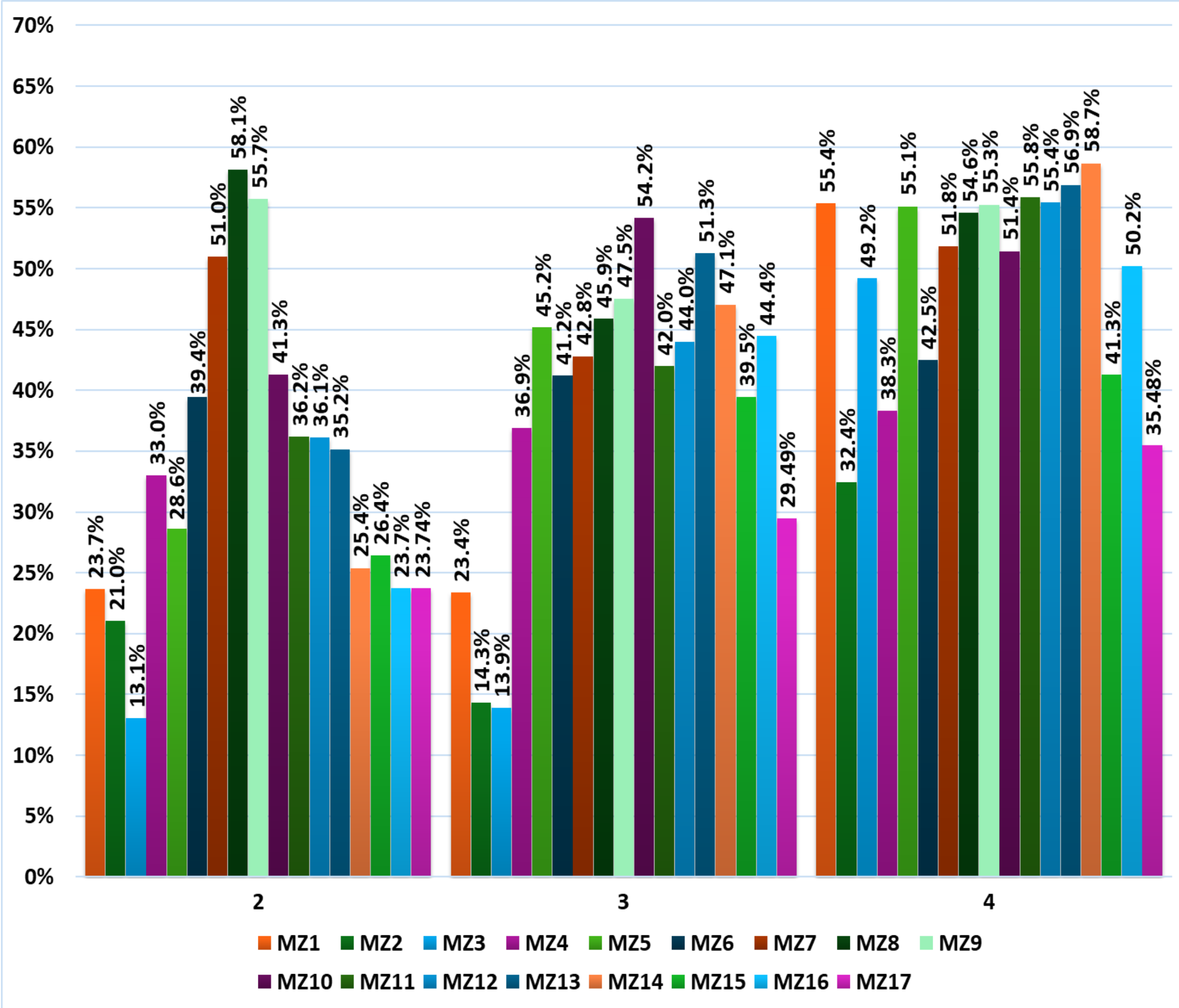

Figure 5. Variance reduction of the mean yield for each management zone scenario and zones.

For yield PC1 (Figure 6), the VR% was also good for most scenarios. For 2 zones, the best combination was the same as the yield mean: MZ8 was the best method, reducing the yield internal variance by 61.7%. For 3 zones, as for the yield mean, the best scenario was MZ10, with the VR% of 61.7%. Also, as for the yield mean, using all filtered variables (MZ14) for 4 zones the VR% was the highest, showing a reduction of 66.8%. Finally, when we compare the VR% of the best scenarios for 4 zones with MZ1 and MZ5, both showed good gains (63.4% and 61.5%), similar to the yield mean. So, based on the VR% alone, it's recommended to use the MZ14 scenario with 4 zones to increase the VR%. The comparable performance of the DEM alone (MZ5) corroborates prior findings, indicating that topography is a primary driver of pedogenetic processes and water-flow dynamics, thereby explaining a large portion of spatial yield variability.

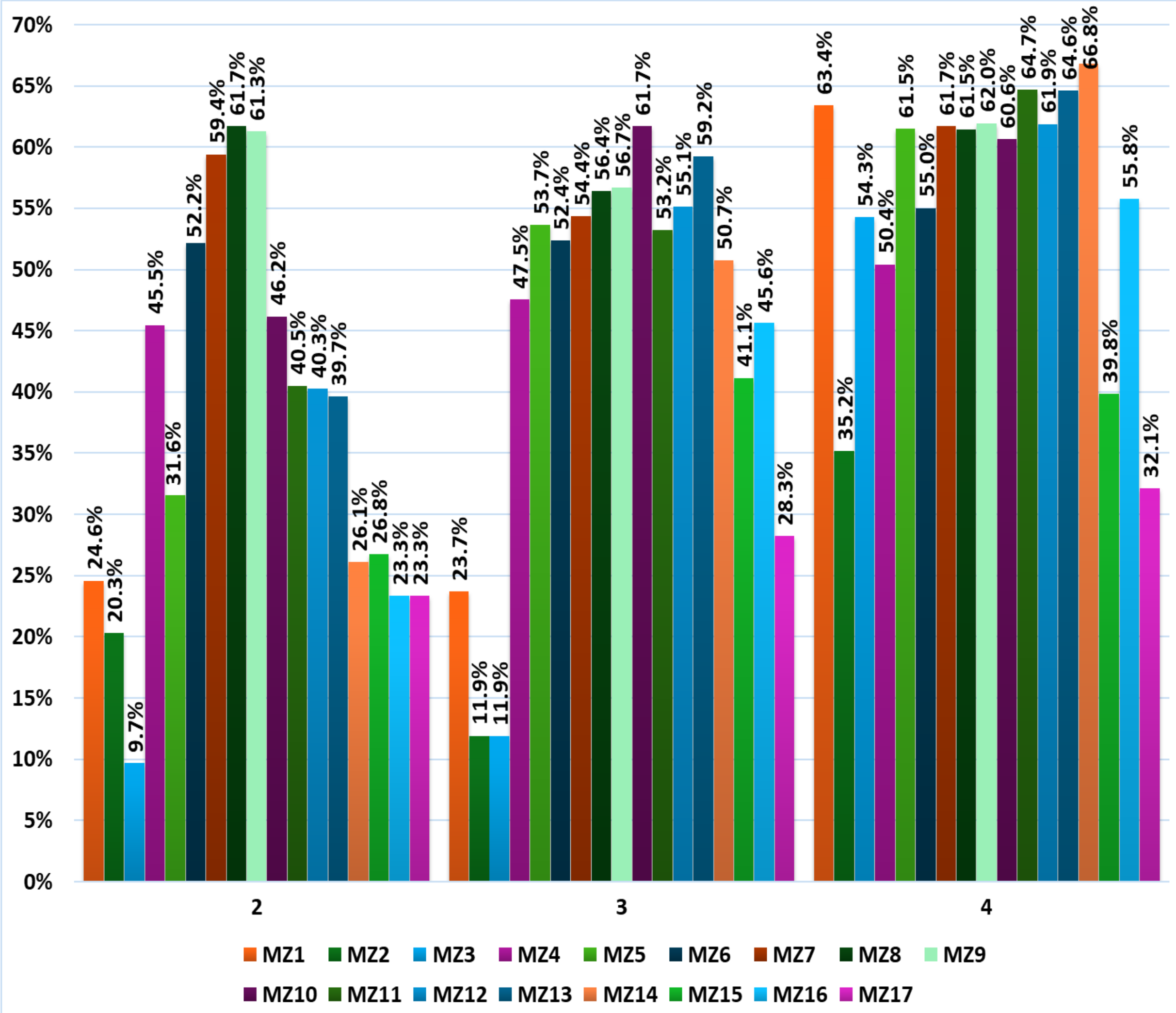

Figure 6. Variance reduction of yield PC1 for each management zone scenario and zones.

Regarding SNVI (Figure 7), the VR% was also good across most scenarios. On the other hand, SVNI had one scenario with a higher VR% for zones 2, 3, and 4. Adopting only ECa75 (MZ6) was the best strategy to reduce the internal variance of the SVNI within zones (61.3%, 66.8%, and 68.8%, respectively). The performance of ECa in predicting the spatial patterns of soil nutritional variability aligns with classical literature (Corwin and Lesch, 2005; Sudduth et al., 2005), which reports relationships between ECa and soil physical and chemical attributes. Also, using all variables without any filtering (MZ1) or using all filtered variables (MZ14) across 4 zones yielded similar gains, with an SVNI VR% of 61.4% and 61.4%, respectively.

Furthermore, to estimate the VR% of soil-plant interaction, the mean VR% was calculated (Figure 8). For 2 zones, selecting ECa75 and DEM (MZ7) can reduce internal variance by 56.6%, representing differences in individuals' VR% for yield mean, yield PC1, and SNVI of 1.11, 0.95, and 0.95, respectively. Furthermore, for 3 zones, MZ10 was the best variable configuration to increase the VR% to 57.3%, representing differences in individuals' VR% for yield mean, yield PC1, and SNVI of 1.06, 0.93, and 1.03, respectively. Finally, for 4 zones, all filtered variables (MZ14) had a VR% of 62.3%, representing individual differences of 1.06, 0.93%, and approximately 1%. However, using all variables (MZ1) had a VR% of 60.0%, representing a good gain, and a difference from MZ14 of 2.3%, which is 3.7% of MZ14. In this case, the differences in the mean VR% for the individual are 1.08, 0.95, and 0.98. Ultimately, the progressive success of the MZ7, MZ10, and MZ14 configurations demonstrates that multi-source data fusion is the optimal approach for defining MZ. Integrating dynamic crop canopy indicators (such as SWIR1 or saturation) with static soil and relief parameters effectively addresses both subsurface limitations and dynamic crop responses, thereby establishing a comprehensive spatial framework (Amaral et al., 2024; Nawar et al., 2017). However, while 4 zones maximize mathematical variance reduction, the 2 or 3 zone configurations (MZ7 or MZ10) often offer a better balance between statistical accuracy and the operational feasibility required for variable-rate applications.

For yield mean, yield PC1, and SNVI, when we removed saturation, DEM, or ECa (MZ15, MZ16, and MZ17) from MZ14, the VR% of the filtered variables for 4 zones reduced in a ratio of 0.51, 0.83, and 0.41, showing the importance to integrate these variables to improve the representation of the spatial variability and reduce the variance of yield and SNVI.

It is important to note that, according to Guastaferro et al. (2010), selecting the number of zones to delineate MZ depends on the user's knowledge. Moreover, there are no strict rules for defining zone sizes (Córdoba et al., 2012), with the choice of the number of zones limited by operational and cost factors; hence, selecting the number of zones must consider practical factors related to the operationalization of management.

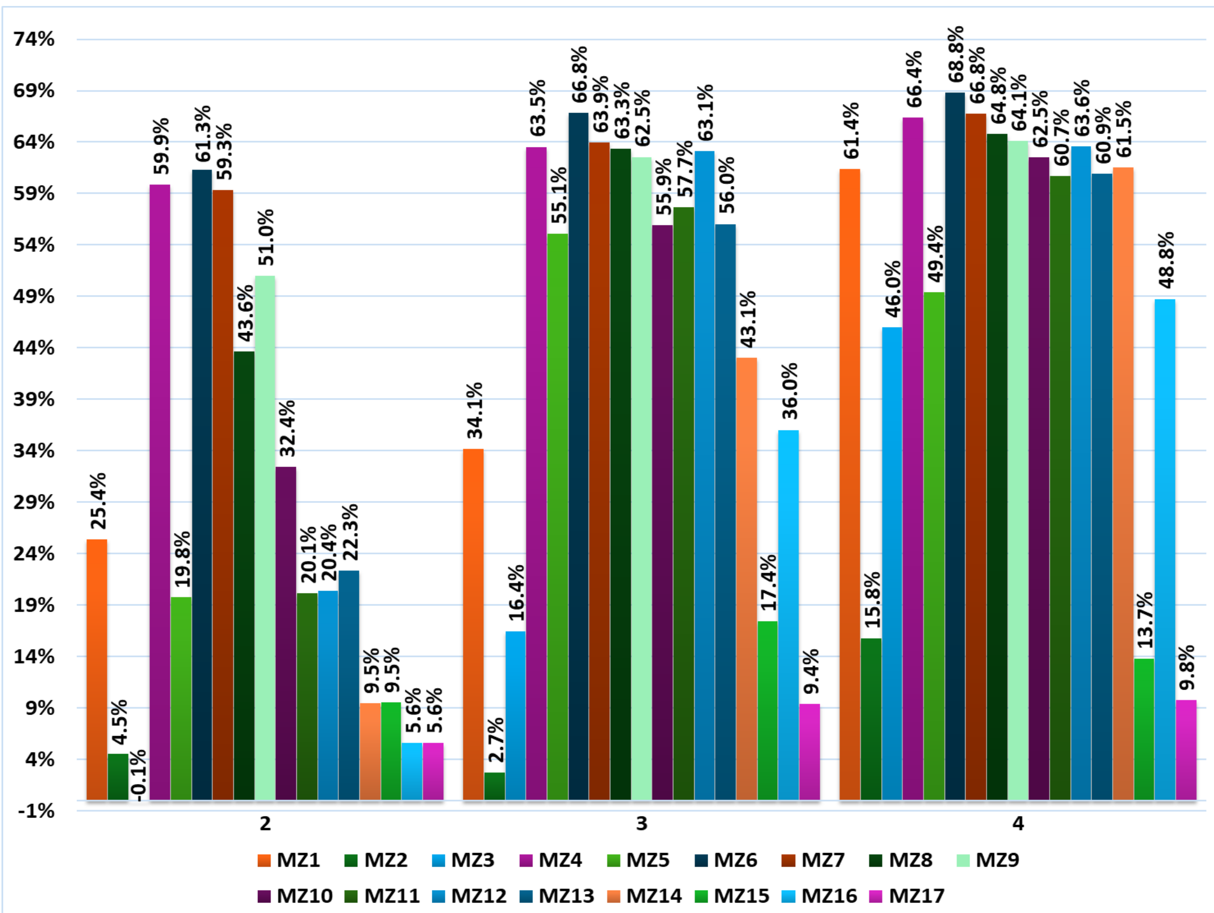

Figure 7. Variance reduction of SNVI for each management zone scenario and zones.

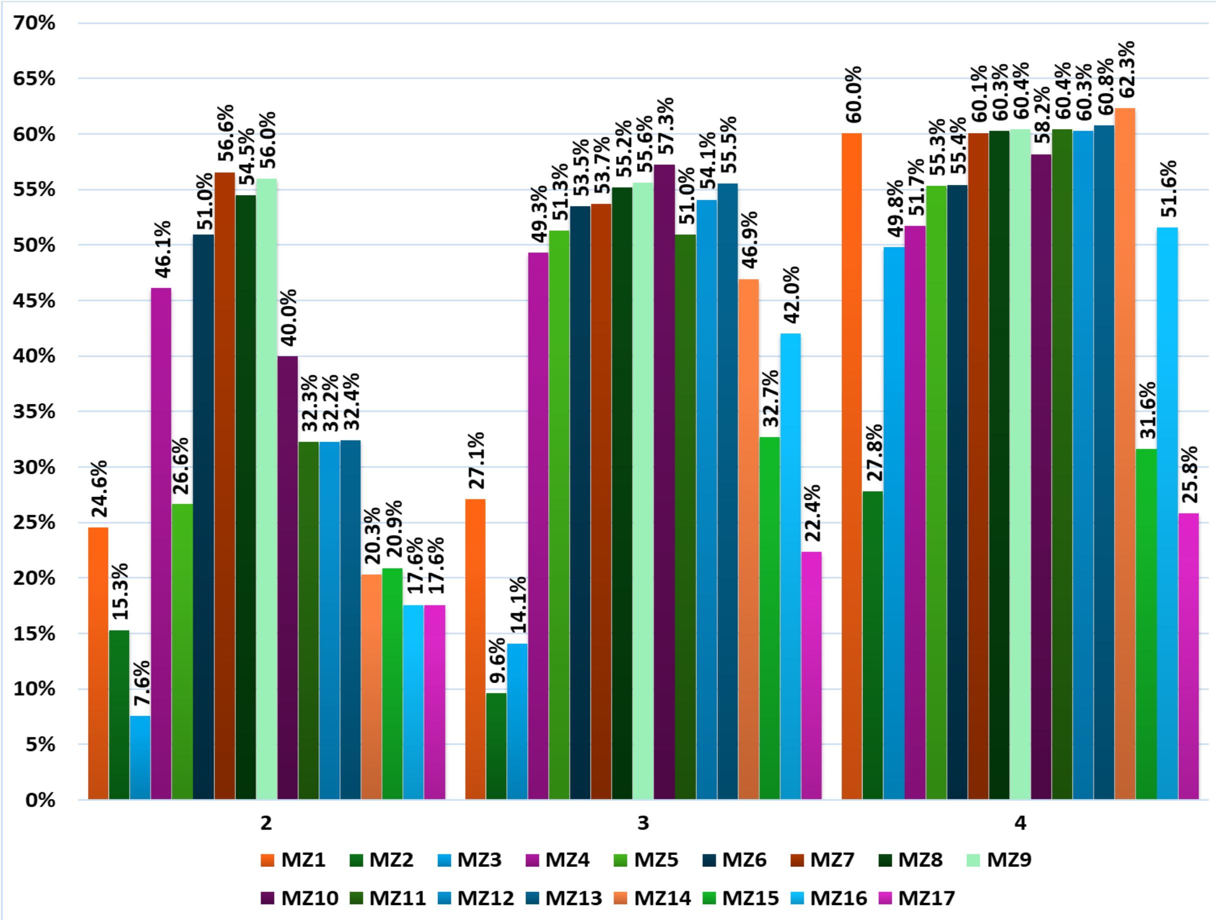

Figure 8. Mean of variance reduction for yield mean, yield PC1, and SNVI for each management zone scenario and zones.

According to figure 8, adopting a strict analysis for 2 and 3 zones, grounded on correlation variables between them and with yield and soil, improved the gains, which is represented for MZ7 (56.6%) and MZ10 (57.3%), respectively. Furthermore, for 4 zones, which allowed using more variables, analyzing significance variables and removing variables with correlation over 0.8 presented the best result, with a VR% of 62.3%. The figure 9 shows how these scenarios represent the area. Therefore, using integrated sensor data can generate MZs with high VR%, being a good approach to represent homogenous zones for both plant and soil information.

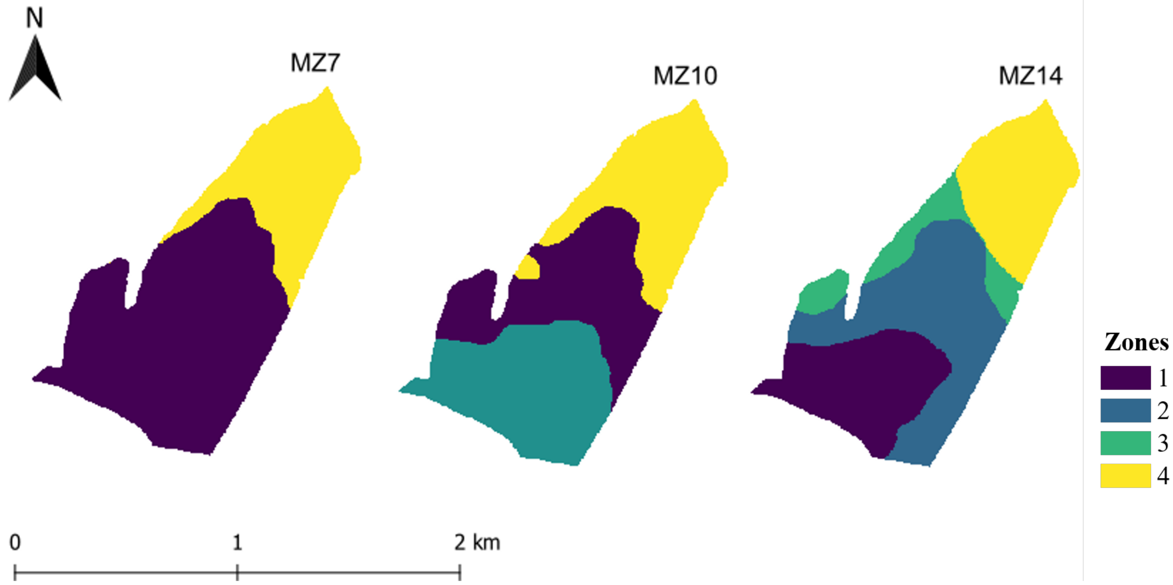

Figure 9. Best zone scenarios for 2 (left), 3 (middle), and 4 (right) zones.

CONCLUSION

This work demonstrates that delineating MZ using different sources of data can improve the quality of the zones, reducing the within-zone variance. Compared to scenarios using only ECa, DEM, or SYSI bands, integrating these different data can improve the VR% for 2, 3, and 4 zones. Also, increasing the number of zones can improve the VR% for most scenarios, except for MZ8 for yield mean and yield PC1 . Additionally, using 2, 3, or 4 zones can minimize the internal variance of yield and SVNI over 50%, but only with 4 zones the VR% was over 60%. Therefore, selecting the number of zones it's an important stage to determine what scenario will be the best. Although it's important to select the number of zones, this study sought to evaluate in general if integrating data from different sensors can minimize the internal variance of the MZ and what is the best combination of data to achieve MZ with low internal variance. Therefore, for this work, the MZ14 scenario in 4 zones was the best to represent the variability of soil and plant, showing a good VR% within-zones.

ACKNOWLEDGMENTS

The authors express their gratitude to the owners and staff of the São José farm for providing access to the research site. Appreciation is also extended to the members of the Interdisciplinary Group on Precision Agriculture Technology (GITAP) for their assistance with soil collection, laboratory analysis, and sensor utilization.

REFERENCES

Adamchuk, V. I., Hummel, J. W., Morgan, M. T., & Upadhyaya, S. K. (2004). On-the-go soil sensors for precision agriculture. Computers and Electronics in Agriculture, 44(1), 71–91.

https://doi.org/10.1016/j.compag.2004.03.002

Bejarano, L. D., Oliveira, A. L. G., Pozzuto, J. V. F., Sánchez, D. C., & Amaral, L. R. (2026). Performance of interpolation methods in digital soil mapping: the influence of data characteristics. Precision Agriculture, 27(1), 10. https://doi.org/10.1007/s11119-025-10311-8

Cherubin, M. R., Damian, J. M., Tavares, T. R., Trevisan, R. G., Colaço, A. F., Eitelwein, M. T., et al. (2022). Precision Agriculture in Brazil: The Trajectory of 25 Years of Scientific Research. Agriculture, 12(11), 1882. https://doi.org/10.3390/agriculture12111882

Córdoba, M. A., Bruno, C. I., Costa, J. L., Peralta, N. R., & Balzarini, M. G. (2016). Protocol for multivariate homogeneous zone delineation in precision agriculture. Biosystems Engineering, 143, 95–107. https://doi.org/10.1016/j.biosystemseng.2015.12.008

Córdoba, M., Balzarini, M., Bruno, C., & Costa, J. L. (2012). Identificación de zonas de manejo sitio-específico a partir de la combinación de variables de suelo. *Ciencia y Tecnología Agropecuaria*, *13*(1), 47-54. https://doi.org/10.21930/rcta.vol13_num1_art:239

Corwin, D. L., & Lesch, S. M. (2005). Apparent soil electrical conductivity measurements in agriculture. Computers and Electronics in Agriculture, 46(1–3), 11–43. https://doi.org/10.1016/j.compag.2004.10.005

Demattê, J. A. M., Fongaro, C. T., Rizzo, R., & Safanelli, J. L. (2018). Geospatial Soil Sensing System (GEOS3): A powerful data mining procedure to retrieve soil spectral reflectance from satellite images. *Remote Sensing of Environment*, *212*, 161–175. https://doi.org/10.1016/j.rse.2018.04.047

Demattê, J. A. M., Rizzo, R., Rosin, N. A., Poppiel, R. R., Novais, J. J. M., Amorim, M. T. A., et al. (2025). A global soil spectral grid based on space sensing. Science of The Total Environment, 968, 178791. https://doi.org/10.1016/j.scitotenv.2025.178791

Dray, S., Saïd, S., & Débias, F. (2008). Spatial ordination of vegetation data using a generalization of Wartenberg's multivariate spatial correlation. Journal of Vegetation Science, 19(1), 45–56. https://doi.org/10.3170/2007-8-18312

Guastaferro, F., Castrignano, A., De Benedetto, D., Sollitto, D., Troccoli, A., & Cafarelli, B. (2010). A comparison of different algorithms for the delineation of management zones. *Precision agriculture*, *11*(6), 600-620. https://doi.org/10.1007/s11119-010-9183-4

Hengl, T., & MacMillan, R. A. (2009). Geomorphometry — A Key to Landscape Mapping and Modelling. In T. Hengl & H. I. Reuter (Eds.), *Developments in Soil Science* (Vol. 33, pp. 433–460). Amsterdam: Elsevier Ltd. https://doi.org/10.1016/S0166-2481(08)00019-6

ISPA. (2024, January). Precision Ag Definition | International Society of Precision Agriculture. *Precision Ag Definition*. https://www.ispag.org/about/definition. Accessed 08 June 2026.

McBratney, A. B., Mendonça Santos, M. L., & Minasny, B. (2003). On digital soil mapping. Geoderma, 117(1–2), 3–52. https://doi.org/10.1016/S0016-7061(03)00223-4

Melo, D. D., Cunha, I. A., & Amaral, L. R. (2025). Precision Zones: An Open-Source QGIS Plugin for Management-Zone Segmentation in Precision Agriculture. *AgriEngineering*, *7*(12), 420. https://doi.org/10.3390/agriengineering7120420

Molin, J. P., Amaral, L. R., & Colaço, A. F. (2015). Agricultura de precisão (1st ed.). São

Paulo: Oficina de textos.

Molin, J. P., & Tavares, T. R. (2019). Sensor Systems for Mapping Soil Fertility Attributes: Challenges, Advances, and Perspectives in Brazilian Tropical Soils. Engenharia Agrícola, 39(Special Issue: Precision Agriculture), 126–147. https://doi.org/10.1590/1809-4430-eng.agric.v39nep126-147/2019

Nawar, S., Corstanje, R., Halcro, G., Mulla, D., & Mouazen, A. M. (2017). Delineation of Soil Management Zones for Variable-Rate Fertilization: A Review. In Advances in Agronomy (Vol. 143, pp. 175–245). Academic Press Inc. https://doi.org/10.1016/bs.agron.2017.01.003

Oldoni, H., Magalhães, P. S. G., Oliveira, A. L. G., Lima, J. P., Figueiredo, G. K. D. A., Moro, E., & Amaral, L. R. (2025). Management zones delineation: a proposal to overcome the crop-pasture rotation challenge. Precision Agriculture, 26(1), 21. https://doi.org/10.1007/s11119-024-10214-0

Pentoś, K., Pieczarka, K., & Serwata, K. (2021). The relationship between soil electrical parameters and compaction of sandy clay loam soil. Agriculture (Switzerland), 11(2), 1–11. https://doi.org/10.3390/agriculture11020114

Peralta, N. R., Costa, J. L., Balzarini, M., Castro Franco, M., Córdoba, M., & Bullock, D. (2015). Delineation of management zones to improve nitrogen management of wheat. Computers and Electronics in Agriculture, 110, 103–113. https://doi.org/10.1016/j.compag.2014.10.017

Peralta, N. R., & Costa, J. L. (2013). Delineation of management zones with soil apparent electrical conductivity to improve nutrient management. Computers and Electronics in Agriculture, 99, 218–226. https://doi.org/10.1016/j.compag.2013.09.014

Pozzuto, J. V. F., Bejarano, L. D., Oldoni, H., & Amaral, L. R. (in press)(2026). Complementarity of proximal and orbital soil sensing for mapping on-farm soil variability. *Precision Agriculture*.

Shirzaditabar, F., & Heck, R. J. (2022). Characterization of soil magnetic susceptibility: a review of fundamental concepts, instrumentation, and applications. Canadian Journal of Soil Science, 102(2), 231–251. https://doi.org/10.1139/cjss-2021-0040

Silvero, N. E. Q., Demattê, J. A. M., Amorim, M. T. A., Santos, N. V. dos, Rizzo, R., Safanelli, J. L., et al. (2021). Soil variability and quantification based on Sentinel-2 and Landsat-8 bare soil images: A comparison. Remote Sensing of Environment, 252, 112117. https://doi.org/10.1016/j.rse.2020.112117

Sudduth, K. A., Kitchen, N. R., Wiebold, W. J., Batchelor, W. D., Bollero, G. A., Bullock, D. G., et al. (2005). Relating apparent electrical conductivity to soil properties across the north-central USA. Computers and Electronics in Agriculture, 46(1-3 SPEC. ISS.), 263–283. https://doi.org/10.1016/j.compag.2004.11.010

Tavares, T. R., Amaral, L. R. do, & Minasny, B. (2025). Applications of soil sensors. In D. C. Weindorf, S. Chakraborty, & B. Li (Eds.), *Unlocking the Secrets of Soil* (pp. 233–254). Summerville: Candice Janco. https://doi.org/10.1016/B978-0-443-29879-0.00005-8